

DYNAMIC STIFFNESS IMPLICATIONS FOR A MULTI-AXIS GRINDING SYSTEM

By

Hodge E. Jenkins¹

Georgia Institute of Technology
The George W. Woodruff School
of Mechanical Engineering
Atlanta, GA 30332-0405

Thomas R. Kurfess²

Georgia Institute of Technology
The George W. Woodruff School
of Mechanical Engineering
Atlanta, GA 30332-0405

Abstract

Operating a machine tool, such as a grinder, so that the spindle speed is at a system natural frequency may be useful as the dynamic stiffness is lower at that frequency and thus may be more tolerant to force variations. It is hoped that a result of this type of operation may produce a better quality surface. In this research the dynamic stiffness of a three-axis grinding system is experimentally determined. Grinding experiments are then conducted to determine the effects of dynamic stiffness on surface finish in terms of the surface profile characteristics. Displacements induced by grinding wheels typically exhibit a once-per-revolution effect. Thus, the first experimental grinding wheel speed (in terms of revolutions per second) is selected by examining the empirical dynamic stiffness data and choosing a resonant frequency (cycles per sec) in the range of achievable grinding wheel speeds (revolutions per second). For comparison a grinding run is performed using a higher grinding wheel speed, where the system dynamic stiffness at the corresponding frequency is larger. Additionally simulations are performed for estimated grinding displacement time-histories, based on wheel speed. Simulated results support the preliminary experimental data, that indicate smoother surfaces result when grinding with rotational speeds corresponding to a natural frequency.

Introduction

Machine tool designers have considered the machine tool to be a static stiffness element, that is a spring. A current and logically accepted practice in designing a machine tool is to make the tool stiffness as large as possible. This is especially true in grinding where normal forces are large. By designing and implementing very high stiffnesses in machines, displacement variations

¹ Author is presently with Lucent Technologies, Bell Laboratories in Norcross, GA.

² Please direct all correspondence to this author.

from the cutting forces are reduced. However, this has created machines that are large in size, weight and cost; and, little consideration is given to exploiting the machine dynamics.

We have considered a necessary alternative to this scenario, a compliant force-controlled grinding system. This type of machine tool design and operation, if successful, can have significant impact on the machine configuration, size, cost and abilities. Multi-axis machine tools are typically more compliant than traditional ones. It is with this in mind that we have begun to investigate dynamic stiffness implications for a multi-axis grinding system.

Dynamic stiffness is the relationship between the applied force and the resulting displacement of a point in a system, and is defined in equation (1) for the frequency domain. Note that the dynamic stiffness, $K_d(s)$, is dependent on the frequency, ω , of the applied force, as well as the system physical constants.

$$K_d(s) = \left. \frac{F(s)}{X(s)} \right|_{s=j\omega} \quad (1)$$

A simple example of dynamic stiffness is a one-degree of freedom mass connected to an anchored spring. When the mass of such system is excited by a sinusoidal force at low frequencies (much less than the natural frequency of the system), the displacement of the mass is primarily governed by the spring, (neglecting friction and damping). Indeed, at near-zero frequencies the system behaves as a spring, as inertial forces are insignificant. As the forcing frequency is increased from a near-zero frequency, approaching the natural frequency of this system, the displacement of the mass is not described by the simple spring relationship, $F = KX$, but by the familiar second order dynamic relationship of equation (2).

$$F(t) = F_o \sin \omega t = Kx(t) + B\dot{x}(t) + M\ddot{x}(t) \quad (2)$$

Applying the Laplace transform to the above equation, in the absence of damping (*i.e.*, $B=0$) and with static equilibrium initial conditions, equation (2) reduces to the form

$$F(s) = KX(s) + s^2MX(s) = K_d(s)X(s) \quad (3)$$

Where the fundamental or natural frequency of the system is

$$\omega_n = \sqrt{K/M} \quad (4)$$

Clearly the mass is part of the system's dynamic stiffness. As such the effective system stiffness is not a constant but a function dependent on the forcing frequency, as seen in equation (5).

$$K_d(s)|_{s=j\omega} = \frac{F(s)}{X(s)}|_{s=j\omega} = K + Ms^2|_{s=j\omega} = K - M\omega^2 \quad (5)$$

If the frequency of the applied force, ω , is increased significantly beyond the fundamental frequency, the resulting dynamic stiffness asymptotically approaches an infinite stiffness value with phase of 180° . As $\omega \gg \omega_n$, the system behaves simply as a mass with an insignificant contribution from the spring. Figure 1 shows a hypothetical dynamic stiffness magnitude curve for a second order system. At the resonant frequency the resulting force of any displacement variation is minimized by the effective lower stiffness of the machine tool.

For the grinder system under study, damping is present to limit the resonance amplitude. The grinder also has many resonant modes. Thus, experimentally derived results are used to determine the dynamic stiffness.

Background

Significance for Machine Tools

Dynamic stiffness is considered to be important in machine tool design for several reasons: 1) quality of the part being machined, 2) machine tool life, 3) repeatability of the part being manufactured. Current machine tool design philosophies target the reduction of tool vibration effects by increasing stiffness and adding damping.

The generally accepted premise in precision machine tool design is that the greater the machine stiffness (and resonant frequency) is, the better each of the aforementioned considerations will be (Chitayat, 1991). However, when forced at higher frequencies, a system natural frequency may be encountered. At this resonant frequency the dynamic stiffness of the system is reduced resulting in a more compliant machine tool. Once the dynamic stiffness of a machine tool is known, questions arise regarding the beneficial application of this knowledge.

Recent experimental research in dynamic stiffness was conducted for a precision lathe (Franse, Roblee, and Modemann, 1991) and precision air bearings (Horikawa, Sato and Shimokohbe, 1992). The objective of the research was to increase dynamic stiffness for precision position control applications, by identifying and avoiding resonant modes.

Grinding Applications

A possible exploitation of a priori knowledge of dynamic stiffness for a grinding system is to operate at a natural frequency (resonant grinding). Force control is important in controlling material removal rates and grinding wheel wear. Research relating material removal rates (MRR)

to grinding process variables such as the normal force has long been established (Hahn and Lindsay, Kurfess, Whitney and Brown 1988, 1990). Recently, it has been shown that surface finish is not simply a function of machine tool rigidity, but it is also a function of how well the normal force is controlled (Nagao and Hatamura, 1993). At a resonant frequency, the system stiffness is relatively low, allowing periodic fluctuations of the grinding wheel (*e.g.*, a high spot) to induce smaller force variations. Thus, resonant mode grinding may be beneficial in maintaining a constant normal force and achieving a smaller surface roughness on the finished part.

Typical grinding applications involve closed-loop servo systems with bandwidths on the order of 10 Hz. Since Grinding wheel speeds are typically 100 Hz and greater, servo control cannot typically compensate for disturbances generated by the grinding wheel. Thus for virtually all machine tools, the dynamic response will be independent of the closed-loop servo system (Ulsoy and Koren 1993, Franse *et al* 1991, Liang 1994, and Jeong and Ro 1993).

The point of this investigation is to determine if operating the grinding wheel at a natural frequency of the system results in improved surface finish, from the increased compliance in the system which cushions the grinding wheel, and lowers the normal force variations. By reducing the variation of the normal force during grinding, material removal should be more constant and machine tool deflections may be predicted more accurately from part to part, improving the repeatability of the resulting part shape. (Alternatively, it is possible that greater variance in tool positions may occur, owing to potential larger displacements from the tool force variations.)

There is a trade-off regarding the benefit obtained from additional compliance. If compliance is too great then the imparted cutting forces and the associated material removal rates may not be acceptable from a cost perspective. Other concerns with the application of resonant mode grinding include phase lag and non-orthogonal modal response. Resonant effects may cause larger displacements and possibly a poorer surface finish. In addition to the magnitude of the dynamic stiffness, the phase is also important. Phase sensitivity is also greatest at the resonance. A phase lag of 180° will cause instabilities associated with resonant modes. Additionally, some modes of the system will be three-dimensional; so, force excitation in one direction may result in a machine tool vibratory response in an orthogonal direction to the normal force. Such a three-dimensional modal response may be coupled to velocity, and can affect the grinding speed and the resulting surface finish (Jenkins, Kurfess and Dorf, 1996).

Resonant Mode Grinding Experiments

Dynamic Stiffness Experiment

Dynamic stiffness of a three-axis prismatic servo stage (at a single position) was determined using a stepped sine sweep shaker test. Figure 2 depicts the servo stage with instrumentation and a shaker. A Wilcoxon Research, model F3, electromagnetic shaker, complete with force sensor and accelerometer was attached to the tool end of the servo stage Z-axis. Both the force transducer and accelerometer measure along the line of action of the shaker. An additional accelerometer (Bruel & Kjaer Type 4369) was used to measure acceleration in directions perpendicular to the line of action of the shaker. An eddy current probe, Kaman model 2400, was also used to measure actual displacements directly for comparison.

The system was tested by shaking along each of the three coordinate axes from the tool end. The shaker and sensors were connected to a Data Physics model DP-420 FFT Analyzer, a PC-based instrument that generates stepped sine output to calculate transfer functions. Two-hundred discrete frequencies from 30 to 5,000 Hz, logarithmically spaced, were sampled. A coherence lower limit of 0.95 was used by the instrument to determine the number of independent data captures for averaging at each frequency. Using this experimental design, the tool-end displacements are determined as a function of the applied force frequency.

Dynamic Stiffness Results

The Fast Fourier Transforms from the input force to the output of the accelerometers and eddy current probe were obtained using stepped sine input. A comparison of the transfer function magnitude plots of the three sensors for the Z-axis stiffness is given in Figure 3. The eddy current sensor exhibits a low signal to noise resolution at the higher frequencies which levels-off after 1,000 Hz. Note however, the plots do reveal a good agreement among the sensors in terms of the relative profile, clearly indicating which frequencies induce relatively lower dynamic stiffness. All the sensors tend to display an asymptotic 40 dB per decade 'roll-up' second-order response for dynamic stiffness; however, the accelerometer data continue to do so at the higher frequencies. The accelerometer data (which has a linear output up to 39 kHz) are used for the determination of the three dimensional dynamic stiffness measurements in this paper.

Figures 4 through 6 plot the three axial stiffnesses for excitation along the X, Y and Z axes, respectively. Note the Z-axis is of particular importance as it is the direction normal to the grinding force. The Z-axis dynamic stiffness data are utilized in the experiment for determining the effect of resonant mode grinding on surface quality. From the figures, it can be seen that there

are several significant resonant frequencies where dynamic stiffness is reduced (*e.g.*, 50, 120, 190 Hz ...).

To demonstrate the effects of the closed-loop servo system on the dynamic stiffness, the acceleration and stiffness magnitudes are plotted as a function of frequency for force excitation and displacement measurement along the X-axis, with the servo power on and off (Figure 7). As expected there is no appreciable difference as the servo system bandwidth is approximately 10 Hz. It is clear from the acceleration versus frequency curve in Figure 7, that there are significant resonant modes at frequencies above 400 Hz. Similar results occur for the Y and Z axes, as all axes were tuned to approximately a 10 Hz bandwidth.

Profile Generation Experiment

To compare the resulting surface finish effects of grinding at a resonant mode, two sets of fixed-depth, constant velocity grinding passes were run on 10 mm thick, 1020 carbon steel bar stock each at different grinding wheel speeds. Additional grinding experiments were also performed on other carbon steels including A2, O1, and 4142 (half hard). The three-axis servo system is equipped with a small grinder and a cup-shaped grinding wheel. The system is depicted in Figure 8 (more detail on the grinding system can be found in Ludwick, Jenkins and Kurfess 1994). Grinder shaft speeds range from 120 to 360 rps, so only resonant modes in this range can be examined. From Figure 6 (stiffness along the vertical Z-axis) it can be seen that a small resonance occurs at about 120 Hz, and the dynamic stiffness is significantly larger at 160 Hz. For the Z-axis, phase is near 100° at 120 Hz.

A flat surface was generated by grinding the specimen smooth in multiple passes, using constant velocity traverse (Y-axis) grinding. The depth of material removed was 100 µm for the soft 1020 steel and 20 µm for all the other harder specimens. One grinding pass was performed with a grinder shaft speed of 120 rps and a traverse speed of 4 mm/s. On a second bar a second grinding pass was performed at 160 rps and a traverse speed of 5.33 mm/s. This maintained the material removed per grinding wheel revolution constant, keeping speeds and feedrates proportional. This ensures that any surface anomaly generated in once per revolution of the grinding wheel, occurs with the same spatial periodicity along the specimen.

Profile Results

Figure 9a shows the resulting surface profile for the two ground specimens using a Talysurf profile measuring instrument. A grind length of 9 mm is shown for each specimen, sampling at every µm. The resolution of the Talysurf is 0.1 µm. Similar data are shown for 30 mm lengths on the A2, O1 and 4142 specimens in Figures 9b, 9c, and 9d, respectively.

Table 1 lists surface profile statistics of the specimens using 9,000 data points for the 1020 steel, and 30,000 data points for the other specimens. Linear trends in the data (flatness errors) are removed for a direct comparison of the statistics. Clearly, from examining the statistics and graphical representation of the profiles, the 120 Hz profile provided a smoother surface in terms of the root mean square value, maximum and minimum for the cases of 1020 and the O1 steels, which are the softer steel specimens with Rockwell C hardnesses below 5. The harder specimens exhibited a different response. The A2 specimen has a Rockwell C hardness of 15, while the 4142 half hard steel specimen has a hardness of 25. A general trend is postulated based on the observations summarized in Table 1: as the specimen hardness increases the effect of resonant mode grinding decreases. In fact the resonant mode produced greater surface roughness on the hardest specimen. More experiments are needed to support this supposition.

Typical power spectral densities (PSD) for the surface profiles are plotted in Figure 10, for the 120 Hz wheel speed and 160 Hz wheel speed for the 1020 steel specimen. The PSD was generated using a 1024 point Hanning window. The first peak in the PSD for the 120 Hz wheel speed case is located approximately 30 mm^{-1} ; this corresponds to inverse of the feed travel per grinding wheel revolution. There is no such peak for the 160 Hz grinding pass, as there is no resonant mode, and the dynamic stiffness is much greater. Both profiles exhibit a resonance at 300 mm^{-1} . The exact nature of this phenomenon is unclear.

Figure 11 represents a time history and PSD for a typical normal grinding force with a grinding wheel speed of 120 Hz. The data are from a normal force regulation plunge grinding, sampling at $445 \text{ } \mu\text{s}$. The 120 Hz resonance and higher harmonics show very distinctly, as peaks on the PSD. This is clearly a result of a once-per-revolution and twice-per-revolution effects of the grinding wheel. These grinding force variations about a fixed value can result from many sources, including any pre-existing surface profile, wheel imbalances, grit release and material build-up.

Model and Simulation

Variations in the surface profile can be attributed to two sources, tool end dynamics and process variations induced by tool dynamics. Profile changes attributable to the process variation (because of a non-uniform force) are secondary, as shown in Appendix A, using a first order, grinding model relating MRR to power. Thus, only tool end dynamics are considered in a dynamic model. This is primarily a vibration problem. A simple model is used to estimate the variations in the grinding normal force as a function of displacement disturbances. Several

assumptions are made, including constant contact between the tool and the workpiece, as well as averaging tool end geometry and dynamics for contact area.

Simulations are performed to compare variations in grinding parameters. An estimated disturbance displacement profile is input to the model. The simulated input disturbance is a linear combination of a 15 μm maximum normally distributed displacement and a sinusoidal displacement (25 μm amplitude) at a frequency matching the grinding wheel speed in revolutions per second. This combination is used in an attempt to simulate local variations from grit release and material build-up, and wheel imbalances. The combination is low-pass filtered at twice the grinder speed (Hz) to estimate the effect of contact area in smoothing the disturbances.

The modeled dynamic system is a second order plant with a natural frequency at 120 Hz (corresponding to the actual system resonance) The modeled spring constant is the measured static stiffness of the actual grinding system. Simulations using this model demonstrate the effects of the second order system with varying grinding speeds.

A summary of the model results for simulated grinding is given in Table 2. As seen by the RMS force value in Table 2, the force variation is smallest when the grinder speed is set at the resonance frequency of 120 rps (Hz). As expected (from equation 5) the dynamic system yielded better results (smaller forces) than a simple massless spring. Also interesting is that the 160 rps wheel speed at feed rates of 4.0mm/s and 5.33 mm/s, produced larger forces as compared to the 120 rps wheel speed case. The two feedrates are used to maintain a constant theoretical surface finish for both test cases.

From a modeling perspective, the surface profile quality is related to maintaining a constant material removal rate. The normal force has been shown to related to the metal removal rate from previous work (Ludwick et al 1994). Using these grinding models in conjunction with resonant mode grinding, demonstrates the advantage of grinding at the resonant frequency.

Conclusions

It has been demonstrated that a precision machine tool should not be thought of as a simple spring. In many cases machine tools cannot be designed to have a first mode beyond the induced forcing frequencies, so stiffness will always be a dynamic property. Characterization of a machine tool process may allow one to take advantage of the dynamic stiffness property.

It also appears that resonant mode grinding may be beneficial in attaining smoother surface finishes in some applications. Although improved surface finish was attained in some of the experiments, further research should be performed to address repeatability. The ground material hardness was correlated to the effectiveness of resonant mode grinding. It is not clear

why this resulted. However, chatter may have been pronounced in the harder materials. Future experiments on larger frame, industrial equipment are also needed at higher frequencies to examine higher resonant modes. Diamond turning machines, for example, can run at higher speeds and may have higher frequency modes excited.

Phase angle of the stiffness should play an important role in the effectiveness of this scheme. Phase lags, of $\sim 100^\circ$ at 160 Hz and $\sim 150^\circ$ for 120 Hz are indicative of the stability margin and may be significant in the resulting surface quality. As grinding is a multi-point machine tool process, with a contact area, averaging of disturbances may attenuate the effect of phase.

An issue associated with a three-axis prismatic servo stage system is that the system natural frequencies are a function of position. Different geometries result in different natural frequencies. Also tool-workpiece interaction may cause variations in the resulting frequencies. These constraints may make it difficult to match frequency variations in modal responses. Real-time frequency identification might be useful as a means to accomplish this.

Clearly more work on the development of a more detailed tool/grinding model, and investigations into issues such as machine stresses and wear should be examined. Also effects of regenerative chatter (self-excitation) might be included to improve the understanding of grinding at resonant frequencies.

Acknowledgments

This work was funded by the National Science Foundation under Grant Numbers DDM-9350159, EEC-9256665, and DDM-9257514. The government has certain rights in this material. Any opinions, findings and conclusions or recommendations are those of the authors and do not necessarily reflect the views of the National Science Foundation.

The authors also wish to thank Dr. J. David Cogdell of The Timken Company for his assistance in obtaining profile data.

References

- Brown, N., 1990, *Optical Fabrication*, MISC4476, Revision 1, Lawrence Livermore Laboratory, Livermore, CA, September.
- Chitayat, A., 1991, "Nanometer X-Y Positioning Stages for Scanning and Stepping," *Microelectronics Manufacturing Technology*, Vol. 14, No. 5, May, pp. 60-4.

- Chung, E.S., Chiou, Y.S., Liang, S.Y., 1993, "Tool Wear And Chatter Detection In Turning Via Time-Series Modeling And Frequency Band Averaging," *Manufacturing Science and Engineering, American Society of Mechanical Engineers, Production Engineering Division*, PED Vol. 64, pp. 351-358.
- Fransé, J., Roblee, J.W., and Modemann, K., 1991, "Dynamic Characteristics of the Lawrence Livermore National Laboratory Precision Engineering Research Lathe," *Precision Engineering*, July, Vol., 13, No. 3, pp. 196-202.
- Hahn, R. S. and Lindsay, R. P., 1971, "Principles of Grinding Part I Basic Relationships in Precision Machining," *Machinery*, July, pp. 55-62.
- Hahn, R. S. and Lindsay, R. P., 1971, "Principles of Grinding Part II The Metal Removal Parameter," *Machinery*, August, pp. 33-39.
- Horikawa, O., Sato, K., Shimokohbe, A., 1992, "An Active Air Journal Bearing," *Nanotechnology*, Vol. 3, No. 2, April, pp. 84-90.
- Jenkins, H.E., Kurfess, T.R., Dorf, R.C., 1996, "Design of a Robust Controller for a Grinding System," *IEEE Transactions on Control Systems Technology*, Vol. 4, No. 1, January, pp. 40-49.
- Jeong, S. and Ro, P.I., 1993, "Cutting Force-Based Feedback Control Scheme for Surface Finish Improvement in Diamond Turning," *American Control Conference*, Vol. 2, pp. 1981-1985.
- Kurfess, T.R., Whitney, D.E., and Brown, M.L., 1988, "Verification of a Dynamic Grinding Model," *Journal of Dynamic Systems, Measurement and Control*, December, Vol. 110, pp. 403-409.
- Liang, S.Y., Perry, S.A., 1994, "In-Process Compensation For Milling Cutter Runout Via Chip Load Manipulation," *Journal of Engineering for Industry*, Vol. 116, No. 2 May, pp. 153-160.
- Ludwick, S.J., Jenkins, H.E., Kurfess, T.R., 1994, "Determination of a Dynamic Grinding Model," *1994 International Mechanical Engineering Congress and Exposition*, DSC-Vol. 55-2, pp. 843-849.
- Ma, Q. and Ro, P. I., 1994, "Use of Force Feedback for Dynamics Error Correction in Diamond Turning For Surface Roughness Improvement," *Proceedings of the ASPE 1994 Annual Meeting*, October 2-7, pp. 37-40.
- Nagao, T. and Hatamura, Y., 1987, "Development Of A Flexible Grinding System With Six-Axis Force Sensor For Curved Surfaces," *CIRP Annals*, Vol. 36, No. 1, pp. 215-218.

- Okazaki, Y., 1988, "A Micro Positioning Tool Post Using a Piezoelectric Actuator for Diamond Turning Machines," *Journal of the Japan Society of Precision Engineering*, Vol. 54, No. 7, July, pp. 1375-80.
- Tonshoff, H. K., Zinngrebe, M., Kemmerling, M., 1986, "Optimization of Internal Grinding by Microcomputer-Based Force Control," *CIRP Annals*, Vol. 35, No. 1, pp. 293-296.
- Tung, E., Tomizuka, M., 1993, "Feedforward Tracking Controller Design Based on the Identification of Low Frequency Dynamics," *Journal of Dynamic Systems, Measurement and Control*, September, Vol. 115, pp. 348-356.
- Ulsoy, A.G., Koren, Y., 1993, "Control of Machining Processes," *Journal of Dynamic Systems, Measurement and Control*, June, Vol. 115, pp. 301-308.

Appendix A: Effect of Process Variations

Nomenclature

A	=	Area of the contact patch between the part and grinding wheel
K_p	=	Coefficient for material removal
Q	=	Material removal rate
\bar{Q}	=	Mean material removal rate
δQ	=	Variational material removal rate
δq	=	Variational material removal rate per area (tool end vertical speed variation)
F_N	=	Normal Force between the part and grinding wheel
\bar{F}_N	=	Mean normal force
δF	=	Variational normal force
k	=	Stiffness
m	=	Mass
V	=	Speed of the cutting surface of the grinding wheel
z	=	Position of the ground surface
z_o	=	Position of the ground surface due to constant dz/dt
δz	=	Variation on position of the ground surface
$\xi(s)$	=	Laplace transform of δq
$v(s)$	=	Laplace transform of δz

Metal removal rates have been described as functions of normal grinding forces by several authors (Hahn and Lindsay, 1972, Brown, 1990). A typical linear model (Ludwick, Jenkins and Kurfess, 1994) is given in the following equation:

$$Q = K_p F_N V \quad (1a)$$

Assuming K_p and V as constant over the range of operation, variational forces and material removal rates may be defined as follows.

$$F_N(t) = \bar{F}_N + \delta F(t) \quad (2a)$$

$$Q(t) = \bar{Q} + \delta Q = K_p V \bar{F}_N + K_p V \delta F \quad (3a)$$

$$\bar{Q} = K_p V \bar{F}_N \quad (4a)$$

$$\delta Q = K_p V \delta F \quad (5a)$$

$$\bar{F}_N = kz_o \quad (6a)$$

Applying Newton's Second Law to the tool end displacement

$$m\ddot{z} = F + kz \quad (7a)$$

Taking the variational component from a quasi equilibrium state

$$\delta F = m\delta\ddot{z} + k\delta z \quad (8a)$$

Applying the Laplace transform to (8a)

$$\xi(s) = \mathcal{L}\{\delta q(t)\} \quad (9a)$$

$$v(s) = \mathcal{L}\{\delta z(t)\} \quad (10a)$$

$$\xi(s) = K_p V \mathcal{L}\{\delta F(t)\} \quad (11a)$$

$$\xi(s) = \frac{K_p V}{A} (k + ms^2)v(s) \quad (12a)$$

Thus from equation (12a) the variational grinding rate (or tool end vertical feedrate variation) is proportional to the dynamic stiffness $(k+ms^2)$ by a constant, $\frac{K_p V}{A}$

In this case a numerical value is found based on the parameters found in (Ludwick, et al, 1994)

$$\frac{K_p V}{A} = \frac{(6(10^{-5})[\text{mm}^2 / \text{N}])(6[\text{m} / \text{s}])}{4l[\text{mm}^2]} = 8.78(10^{-6})[\text{m} / (\text{sN})] \quad (13a)$$

This is a very small number. So unless $(k+ms^2)$ is of a very large magnitude the variational displacement will be small. At the resonant mode ($s = j\sqrt{k/m}$) the value $(k+ms^2)$ is small.

$$\text{thus } \lim_{s \rightarrow j\sqrt{k/m}} (k + ms^2) \rightarrow 0 \quad (14a)$$

the result of equations (12a), (13a) and (14a) implies that at resonance

$$\xi(s) \rightarrow 0 \Rightarrow \delta q \rightarrow 0 \quad (15a)$$

Thus the dynamics of the grinding wheel dominate over the variations of the grinding process, in terms of the tool end position and resulting surface profile. This signifies that it may be obtained by beneficial to employ resonant mode grinding.

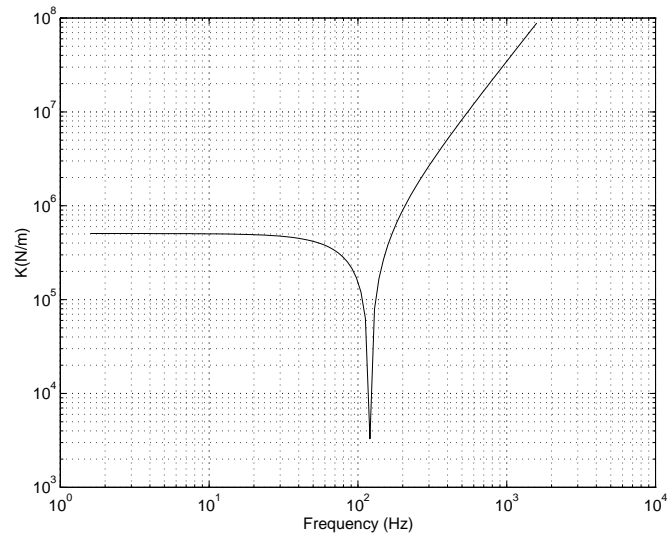


Figure 1. Typical Second Order System Dynamic Stiffness Magnitude.

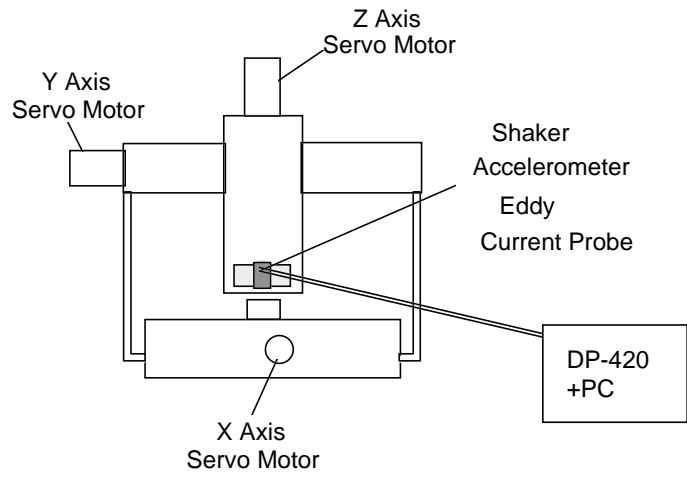


Figure 2. System Schematic For Testing.

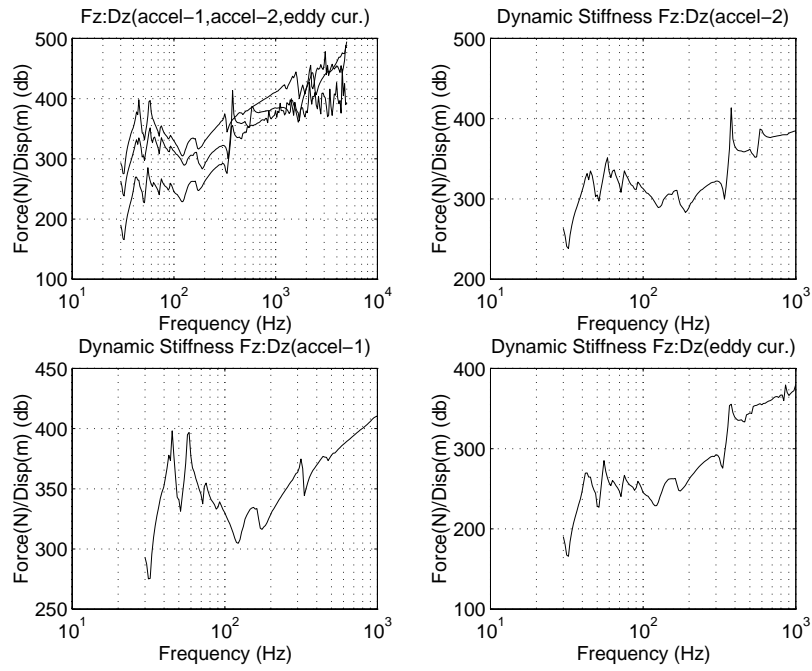


Figure 3. Three Sensor Response for Dynamic Stiffness of Tool End for Force Excitation Along the Z-axis.

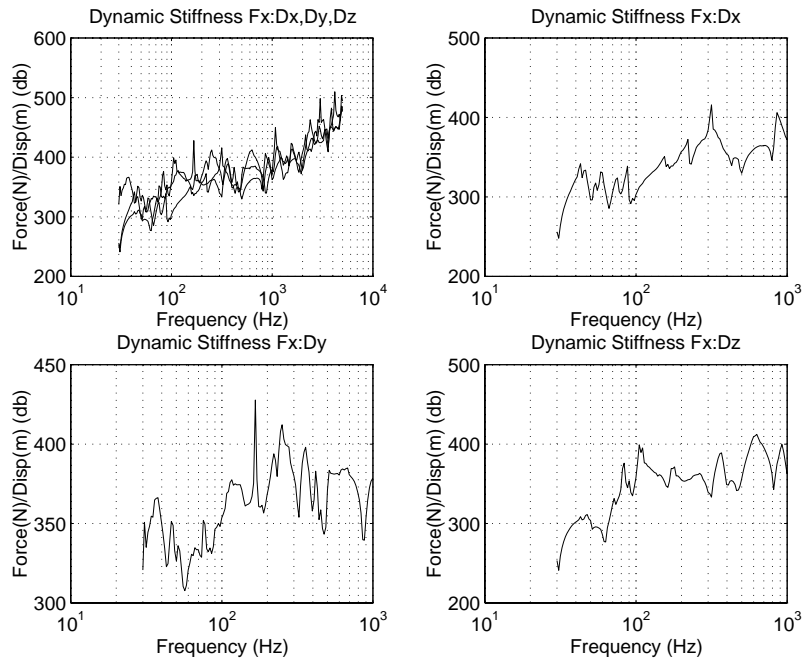


Figure 4. Dynamic Stiffness of Tool End for Force Excitation Along the X-axis.

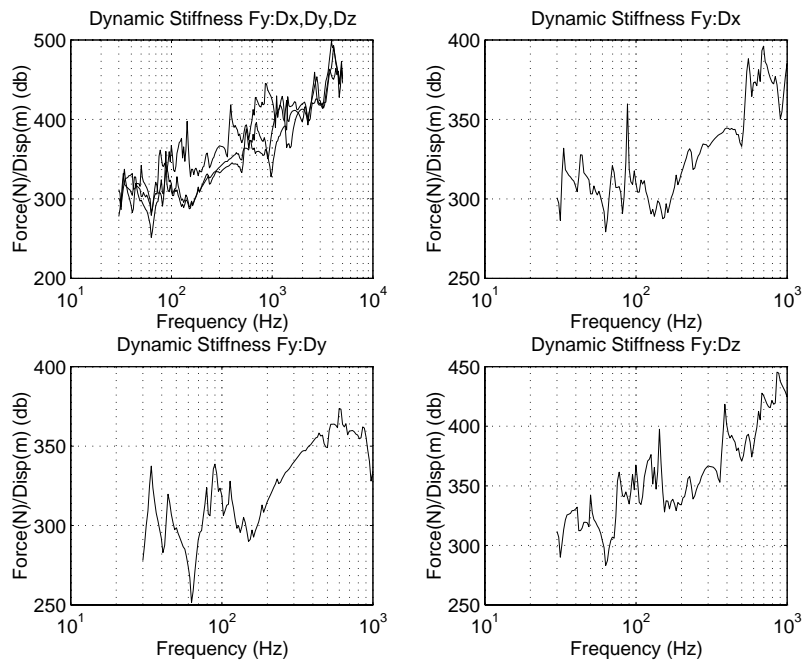


Figure 5. Dynamic Stiffness of Tool End for Force Excitation Along the Y-axis.

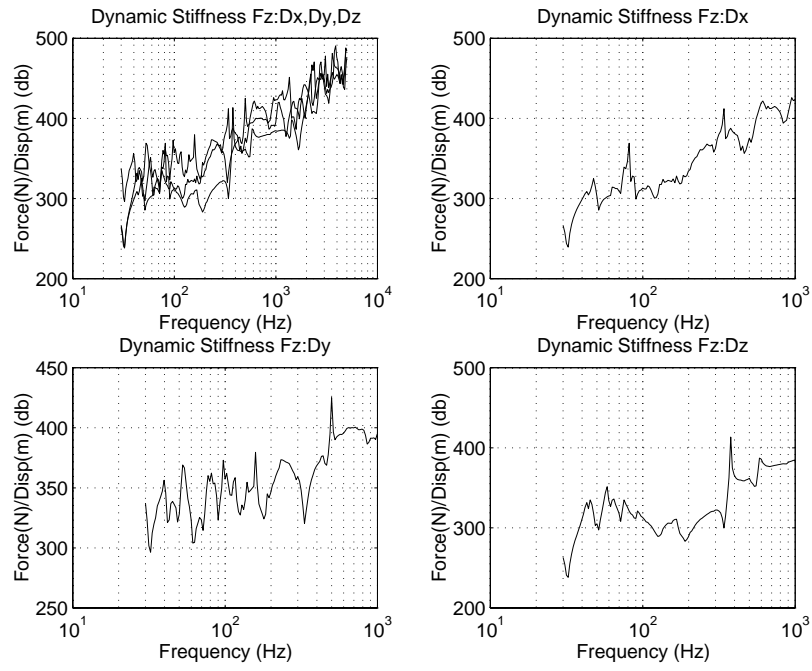


Figure 6. Dynamic Stiffness of Tool End for Force Excitation Along the Z-axis.

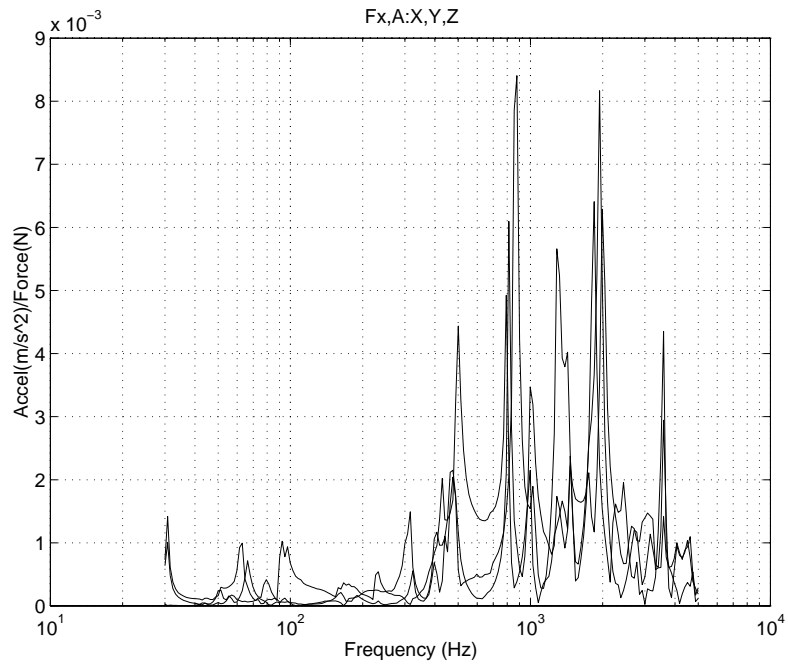


Figure 7. Comparison of Response with Servo Power On and Off.

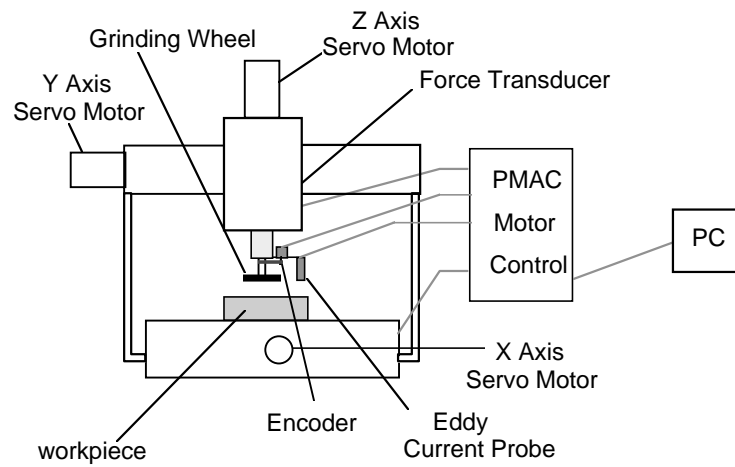


Figure 8. System Schematic for Grinding.

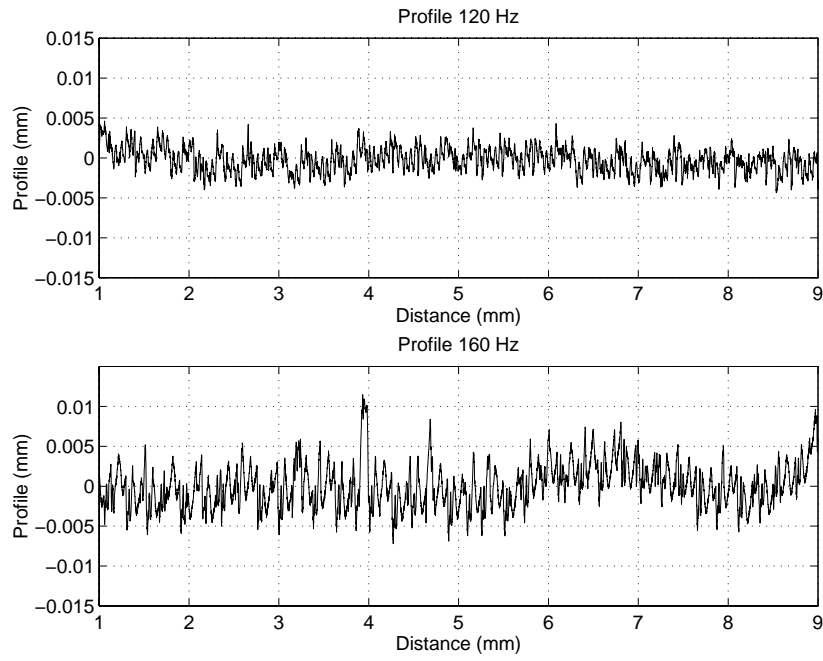


Figure 9a. Surface Profiles Along the Grinding Trajectory (1020 steel).

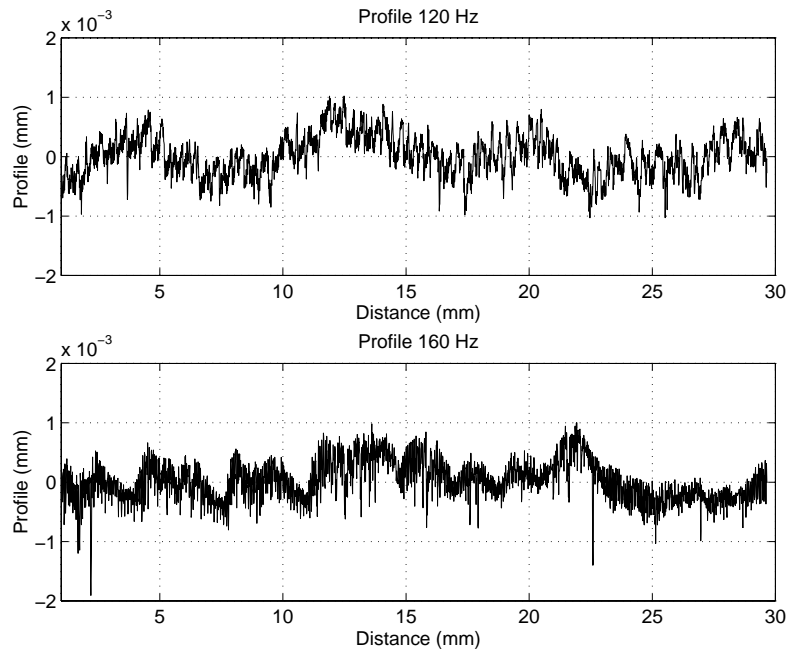


Figure 9b. Surface Profiles Along the Grinding Trajectory (A2 steel).

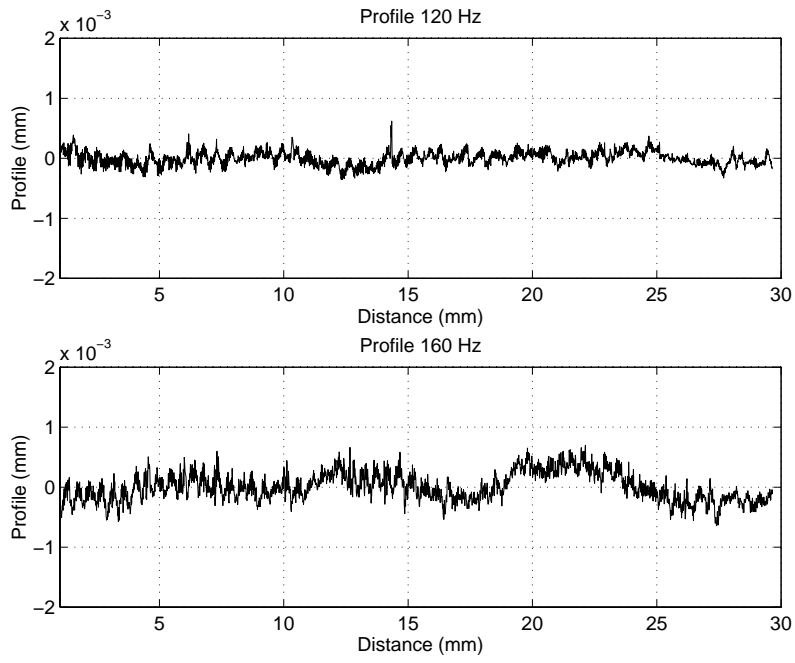


Figure 9c. Surface Profiles Along the Grinding Trajectory (O1 steel).

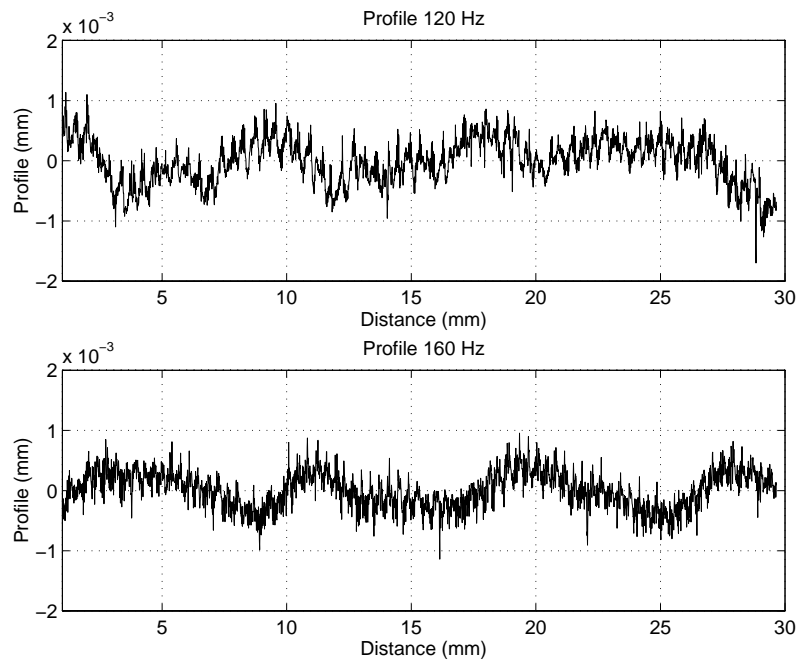


Figure 9d. Surface Profiles Along the Grinding Trajectory (4142 steel).

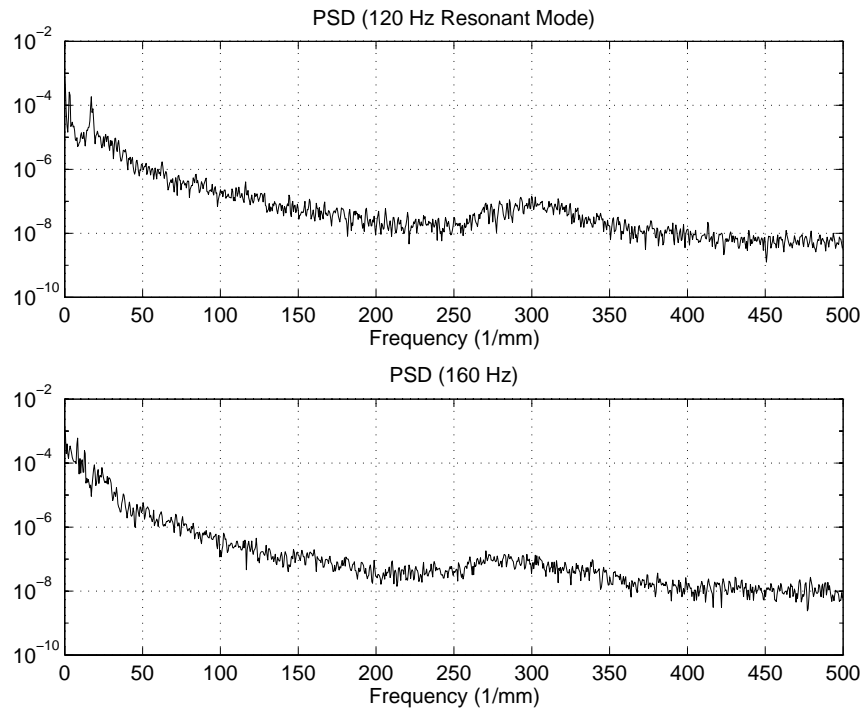


Figure 10. Power Spectral Density of the Ground Surface Using a 1024 Point Hanning Window with Overlap.

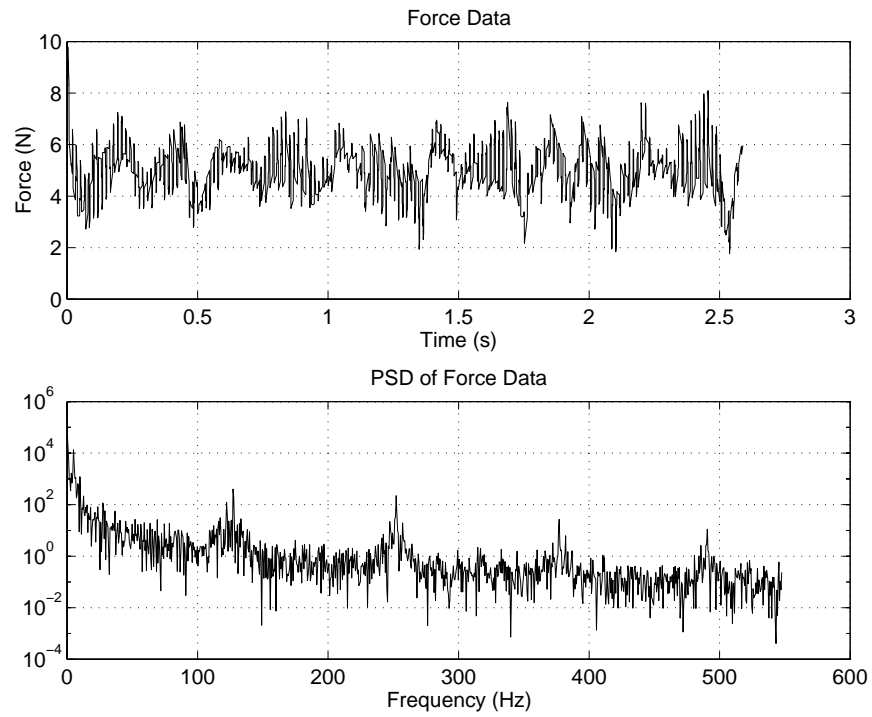


Figure 11. Normal Grinding Force and Power Spectral Density at 120 Hz Wheel Speed.

Table 1. Resulting Surface Profile Statistics

Resulting Surface Statistic	Wheel Speed 120 rps(resonant)	Wheel Speed 160 rps	Ratio: 120 rps /160 rps
1020 carbon steel			
RMS. value (mm)	0.001603	0.002734	59%
Max. (mm)	0.005244	0.011456	46%
Min. (mm)	-0.004350	-0.007198	60%
O1			
RMS. value (mm)	0.000122	0.000241	51%
Max. (mm)	0.000720	0.000832	87%
Min. (mm)	-0.000463	-0.000731	63%
A2			
RMS. value (mm)	0.000357	0.000351	101%
Max. (mm)	0.001105	0.001163	95%
Min. (mm)	-0.001121	-0.001957	57%
4142			
RMS. value (mm)	0.000376	0.000321	117%
Max. (mm)	0.001145	0.001107	103%
Min. (mm)	-0.001727	-0.001150	150%

Table 2. Simulated Variational Force Results Subject to Simulated Wheel Variational Displacements

	Case 1	Case 2	Case 3	Case 4	Case 5
Speed (rps)	120*	120	160	160	60
Feed (mm/s)	4	4	5.33	4	4
Stiffness	Dynamic	Static	Dynamic	Dynamic	Dynamic
RMS. (N)	2.42	4.28	5.53	5.98	3.12
Max.(N)	9.11	8.38	18.37	16.30	5.76
Min. (N)	-10.48	-9.10	-21.77	-20.72	-5.73
Stand. Dev. (N)	0.0165	0.098	0.053	0.034	0.093

* Resonant

Figure Captions

Figure 1. Typical Second Order System Dynamic Stiffness Magnitude.

Figure 2. System Schematic For Testing.

Figure 3. Three Sensor Response for Dynamic Stiffness of Tool End for Force Excitation Along the Z-axis.

Figure 4. Dynamic Stiffness of Tool End for Force Excitation Along the X-axis.

Figure 5. Dynamic Stiffness of Tool End for Force Excitation Along the Y-axis.

Figure 6. Dynamic Stiffness of Tool End for Force Excitation Along the Z-axis.

Figure 7. Comparison of Response with Servo Power On and Off.

Figure 8. System Schematic for Grinding.

Figure 9a. Surface Profiles Along the Grinding Trajectory (1020 steel).

Figure 9b. Surface Profiles Along the Grinding Trajectory (A2 steel).

Figure 9c. Surface Profiles Along the Grinding Trajectory (O1 steel).

Figure 9d. Surface Profiles Along the Grinding Trajectory (4142 steel).

Figure 10. Power Spectral Density of the Ground Surface Using a 1024 Point Hanning Window with Overlap.

Figure 11. Normal Grinding Force and Power Spectral Density at 120 Hz Wheel Speed.

Table 1. Resulting Surface Profile Statistics

Table 2. Simulated Variational Force Results Subject to Simulated Wheel Variational Displacements